Dynamic Model Identification via Hankel Matrix Fitting: Synchronous Generators and IBRs

Abdullah Alassaf
Department of Electrical Engineering
University of South Florida
Tampa, FL
alassaf@usf.edu

Lingling Fan
Department of Electrical Engineering
University of South Florida
Tampa, FL
linglingfan@usf.edu

***Abstract*—This paper presents time-domain measurement data-based dynamic model parameter estimation for synchronous generators and inverter-based resources (IBRs). While prediction error method (PEM) is a well-known and popular method, it requires a good initial guess of parameters which should be in the domain of convergence. Recently, the system identification community has made significant progress in improving the PEM method by taking into consideration of the characteristics of the low-rank data Hankel matrix. In turn, an estimation problem can be formulated as a rank-constraint optimization problem, and further a difference of convex programming (DCP) problem. This paper adopted the data Hankel matrix fitting strategy and developed the problem formulation for the parameter estimation problems for synchronous generators and IBRs. These two examples are presented and the results are satisfying.**

***Index Terms*—Dynamical parameter identification, synchronous generators, inverter-based resources.**

I. Introduction

SYNCHRONOUS generators and inverter-based resources (IBRs) are two major types of resources in power grids. Specifically, IBRs' control structures and parameters are proprietary information. In the current practice of grid industry, generic dynamic models with assumed model structures are used for dynamic assessment, e.g., [1], [2]. How to configure the model parameters using measurement data is of practical importance. For synchronous generators, finding parameters from experiment data has a long and rich history. IEEE standard 115, has a section devoted to identifying various reactances (synchronous, transient, and subtransient) and time constants (open-circuit, short-circuit, transient, and subtransient) through experiments [3]. Furthermore IEEE standard 115A provides a more accurate procedure to identify q-axis quantities through standstill frequency response tests [4]. Those tests have to be conducted offline and are expensive.

The goal of this paper is to design a method to identify model parameters based on time-domain measurement data obtained during online operation. In general, estimating dynamic model parameter for a model with a known structure is termed as gray-box model identification [5] and the most popular method is the PEM method [6]. The PEM method directly uses the input-output time-domain data to identify the parameters [6]. It essentially solves a nonlinear programming problem. Convergence is an issue. In addition, a solution of local optimum can result in a poor matching degree of measured data and its estimation. Another well-known method, Kalman filter, which has been applied for generator parameter estimation in the literature, e.g., [7], [8], suffers the same issues.

Recently, the system identification community has made significant progress in improving the PEM method by taking into consideration of the characteristics of the low-rank data Hankel matrix. In turn, the estimation problem can be reformulated as a rank-constraint optimization problem with a matrix as the decision variable to fit the Hankel matrix formed from the measurement data. This problem can be further formulated as a DCP problem with the objective of minimizing the weighted sum of the nuclear norm of the matrix decision variable and the sum of its first n singular values (where n is the model order) [9], [10]. This paper designs the Hankel matrix fitting-based estimation formulation and solving algorithms for parameter estimation of synchronous generators and IBRs.

For a synchronous generator represented by a second-order dynamic model, this method can accurately estimate the damping coefficient, the machine inertia, and the synchronizing torque coefficient. For an IBR represented by a fourth-order model, this method is able to identify five parameters of the inverter control model accurately.

This paper is organized as follows. Section II presents the gray-box model identification problem formulation. Section III applies the method to the two examples, and Section IV concludes the paper.

II. Hankel Data Matrix-Based Gray-box Model Identification

We start from a nth-order continuous-time state-space model expressed as follows. It has m input and p outputs.

$$\begin{aligned} x(t) &= Ax(t) + Bu(t), \\ y(t) &= Cx(t) + Du(t), \end{aligned} \tag{1}$$

where $A \in \mathbb{R}^{n\times n}$, $B \in \mathbb{R}^{n\times m}$, $C \in \mathbb{R}^{p\times n}$, and $D \in \mathbb{R}^{p\times m}$ are the dynamical system matrix, the input matrix, the output

This work is supported in part by NSF grant #2103480 "Dynamic Model Identification for Inverter-Based Resources".

978-1-6654-9921-7/22/$31.00 ©2022 IEEE

matrix, and the feedthrough matrix, respectively. In many engineering applications, discrete-time state-space models are more often used. The discrete-time state-space model presented is as follows.

$$\begin{aligned} x[kT+T] &= A_d x[kT] + B_d u[kT], \\ y[kT] &= C_d x[kT] + D_d u[kT], \end{aligned} \tag{2}$$

where T is the sampling period and k is the sample number. Many methods accurately convert a continuous-time state-space form to a discrete-time state-space form [11, Chapter 2]. Among the numerical integration methods, Forward-Euler approximation is convenient in parameter identification because it retains the system original structure. If Forward-Euler rule is adopted, the matrices in continuous time domain and discrete time domain are related as follows.

$$A_d = AT + I,\ B_d \ = BT,\ C_d = C,\ D_d \ = D, \tag{3}$$

where I is the identity matrix. The conversion accuracy increases with the sampling period, T, decreasing.

Assume that the feedthrough matrix $D = 0$ and the system matrices are affine towards the parameter vector $\theta \in \mathbb{R}^l$.

$$\begin{aligned} A(\theta) &= A_0 + \sum_{i=1}^{l} A_i \theta_i,\ B(\theta) \ = B_0 + \sum_{i=1}^{l} B_i \theta_i, \\ C(\theta) &= C_0 + \sum_{i=1}^{l} C_i \theta_i, \end{aligned} \tag{4}$$

Assume that impulse response data are available. The gray-box model identification may utilize the low-rank property of the data Hankel matrix formed by the impulse response data and formulate a rank-constraint problem to be solved via DCP.

A. Optimization problem formulation

The optimization problem aims to identify the model parameters by matching the measured impulse response with the impulse response of the parametrized model. The system impulse response measurements, also called Markov parameters, are equivalent to $M_i = C_d(A_d)^i B_d$ for $i = 0, 1, \ldots, R$, where R is the number of the total impulse samples.

The Markov parameters are aggregated in a block Hankel matrix:

$$H^*_{v,h} = \begin{bmatrix} M_0 & M_1 & \cdots & M_{h-1} \\ M_1 & M_2 & \cdots & M_h \\ \vdots & \vdots & \ddots & \vdots \\ M_{v-1} & M_v & \cdots & M_{v+h-2} \end{bmatrix}, \tag{5}$$

where the subscripts v and h represent the number of block rows and columns, respectively. Each of them has to be greater than or equal the system order, n. The outputs of the parameterized system are also collected and formed in a block Hankel matrix.

Solving the following optimization problem may lead to the unknown parameters

$$\begin{aligned} &\min_{\theta} \left\| H^*_{v,h} - H_{v,h}(\theta) \right\|_F^2 \\ &\text{s.t.} \\ &H_{v,h}(\theta) = \\ &\begin{bmatrix} C_d(\theta)B_d(\theta) & \cdots & C_d(\theta)A_d^{h-1}(\theta)B_d(\theta) \\ \vdots & \ddots & \vdots \\ C_d(\theta)A_d^{v-1}(\theta)B_d(\theta) & \cdots & C_d(\theta)A_d^{v+h-2}(\theta)B_d(\theta) \end{bmatrix}. \end{aligned} \tag{6}$$

This is a nonlinear programming problem and it is difficult to find the global solution.

B. Rank-Constraint Reformulation

The matrix $H_{v,h}(\theta)$ is low-rank, and it can be factorized as follows

$$\begin{aligned} H_{v,h}(\theta) = &\underbrace{\begin{bmatrix} C_d(\theta) \\ C_d(\theta)A_d(\theta) \\ \vdots \\ C_d(\theta)A_d^{v-1}(\theta) \end{bmatrix}}_{\mathcal{O}_v(\theta)} \\ &\times \underbrace{\begin{bmatrix} B_d(\theta) & A_d(\theta)B_d(\theta) & \cdots & A_d^{h-1}(\theta)B_d(\theta) \end{bmatrix}}_{\mathcal{C}_h(\theta)}, \end{aligned} \tag{7}$$

where $\mathcal{O}_v(\theta)$ and $\mathcal{C}_h(\theta)$ are the extended observability and controllability matrices, respectively. To differentiate between the $H_{v,h}(\theta)$ original and low-rank structures, the low-rank structure is denoted as X so that $X = \mathcal{O}\mathcal{C}$. Next, two variable matrices are introduced to represent the shift property of $\mathcal{O}_v(\theta)$ and $\mathcal{C}_h(\theta)$, respectively.

$$\begin{aligned} \overline{\mathcal{O}}_v(\theta) &= \begin{bmatrix} \mathcal{O}_v(p+1:vp,:) \\ C_d(\theta)A_d^v(\theta) \end{bmatrix}, \\ \overline{\mathcal{C}}_h(\theta) &= \begin{bmatrix} \mathcal{C}_h(:, m+1:hm) & A_d^h(\theta)B_d(\theta) \end{bmatrix}. \end{aligned} \tag{8}$$

$\overline{\mathcal{O}}_v(\theta)$ and $\overline{\mathcal{C}}_h(\theta)$ respectively hold the relationship of $\overline{\mathcal{O}}_v(\theta) = \mathcal{O}_v(\theta)A_d(\theta)$ and $\overline{\mathcal{C}}_h(\theta) = A_d(\theta)\mathcal{C}_h(\theta)$. The bilinearity of these variables can now be transformed into a rank constraint. As a result, the following problem is formed in [9]:

$$\begin{aligned} &\min_{\theta,\mathcal{O},\mathcal{C},\overline{\mathcal{O}},\overline{\mathcal{C}},X,\bar{A}} \ \|H^*_{v,h} - X\|_F^2 \\ &\text{s.t. } \operatorname{rank} \underbrace{\begin{bmatrix} X & \mathcal{O} & \overline{\mathcal{O}} \\ \mathcal{C} & I_n & A_d(\theta) \\ \overline{\mathcal{C}} & A_d(\theta) & \bar{A} \end{bmatrix}}_{Z} = n, \\ &\mathcal{O}(1:p,:) = C_d(\theta), \\ &\overline{\mathcal{O}}(1:(v-1)p,:) = \mathcal{O}(p+1:vp,:), \\ &\mathcal{C}(:,1:m) = B_d(\theta), \\ &\overline{\mathcal{C}}(:,1:(h-1)m) = \mathcal{C}(:,m+1:hm), \end{aligned} \tag{9}$$

where $\bar{A} = A_d^2(\theta)$. This rank-constraint problem will be solved by DCP in the following subsection.

C. Difference of Convex Programming

The truncated nuclear norm method gives the ability to replace the rank constraint in (9) by the following

$$\|Z\|_* - f_n(Z) = 0, \tag{10}$$

where $\|\cdot\|_*$ is the nuclear norm and $f_n(Z) = \sum_{i=1}^{n} \sigma_i(Z)$. f_n is the sum of the largest n singular values, σ. The nuclear norm and $f_n(Z)$ are all convex in the minimization variables. It can be solved by sequence iteration.

At every jth iteration, the Singular Value Decomposition (SVD) is implemented on Z:

$$Z^j = \begin{bmatrix} U_1^j & U_2^j \end{bmatrix} \begin{bmatrix} S_1^j & \\ & S_2^j \end{bmatrix} \begin{bmatrix} V_1^{j,T} \\ V_2^{j,T} \end{bmatrix}, \tag{11}$$

where U_1^j and $V_1^{j,T}$ denote the n truncated left and right singular matrices, respectively.

$$\begin{aligned} \min_{\theta,\mathcal{O},\mathcal{C},\overline{\mathcal{O}},\overline{\mathcal{C}},X,\bar{A},Z} \quad & \|H_{v,h}^* - X\|_F^2 + \lambda \left(\|Z\|_* - \operatorname{tr}\left(U_1^{j,T} Z V_1^j \right) \right) \\ \text{s.t.} \quad & Z = \begin{bmatrix} X & \mathcal{O} & \overline{\mathcal{O}} \\ \mathcal{C} & I_n & A_d(\theta) \\ \overline{\mathcal{C}} & A_d(\theta) & \bar{A} \end{bmatrix}, \\ & \mathcal{O}(1:p,:) = C_d(\theta), \\ & \overline{\mathcal{O}}(1:(v-1)p,:) = \mathcal{O}(p+1:vp,:), \\ & \mathcal{C}(:,1:m) = B_d(\theta), \\ & \overline{\mathcal{C}}(:,1:(h-1)m) = \mathcal{C}(:,m+1:hm), \end{aligned} \tag{12}$$

where $\lambda > 0$ is a penalty parameter. (12) is a convex programming problem. Also, at the start of the iteration process, the n truncated left and right singular matrices are assumed as zero.

III. Case Studies

This section presents and discusses the implementation of the gray-box algorithm on a single-machine infinite-bus (SMIB) model and an analytical model of grid-integrated IBR. For all the following case studies, the penalty parameter is set to 0.001. The simulations are computed in MATLAB using CVX toolbox [12].

A. Single-Machine Infinite-Bus (SMIB)

The system is shown in Fig. 1, and its state-space model is as follows.

$$\begin{bmatrix} \Delta\dot{\delta} \\ \Delta\dot{\omega} \end{bmatrix} = \underbrace{\begin{bmatrix} 0 & 1 \\ -\frac{K_s\omega_0}{2H} & -\frac{D}{2H} \end{bmatrix}}_{A} \begin{bmatrix} \Delta\delta \\ \Delta\omega \end{bmatrix} + \underbrace{\begin{bmatrix} 0 \\ \frac{\omega_0}{2H} \end{bmatrix}}_{B} \Delta T_\mathrm{m}, \tag{13}$$

where

$$K_\mathrm{s} = \frac{V_T V_\infty \cos\delta}{X_{eq}}. \tag{14}$$

$\Delta\delta$ and $\Delta\omega$ are the deviations of the generator rotor angle in rad and speed in rad/s, respectively. The system nominal angular frequency is $\omega_\mathrm{o} = 2\pi f$, where f is the system frequency (60 Hz). ΔT_m is the mechanical torque, and D is the damping coefficient that is set to 1. The machine inertia H is 3.5 sec. The equivalent system reactance is $X_{eq} = X'_d + X_T + X_L = 0.1033$ pu. K_s is the synchronizing torque coefficient, and it is computed at its equilibrium to be 0.7819. For more details please refer to [13].

TABLE I: SMIB Parameters.

Parameter	Actual	Estimated
θ_1	-0.4205	-0.4211
θ_2	0.9965	0.9986
θ_3	0.5380	0.5387

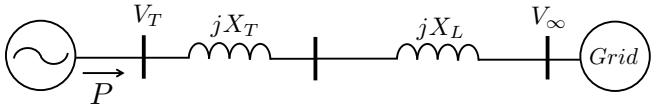

Fig. 1: Single-machine infinite-bus system.

1) Model Identification: The following parameterization structure helps to detect D, H, and K_s.

$$\begin{bmatrix} \Delta\dot{\delta} \\ \Delta\dot{\omega} \end{bmatrix} = \underbrace{\begin{bmatrix} 0 & 1 \\ \theta_1 & \theta_2 \end{bmatrix}}_{A} \begin{bmatrix} \Delta\delta \\ \Delta\omega \end{bmatrix} + \underbrace{\begin{bmatrix} 0 \\ \theta_3 \end{bmatrix}}_{B} \Delta T_\mathrm{m}. \tag{15}$$

The above system's impulse response are shown in Fig. 2 (solid line) and are used for the identification process. The sampling step $T = 0.01$ s. A Hankel data matrix is formed using the measurement data with 10 row blocks and 90 column blocks. After applying the algorithm, the global solution is achieved in 9 iterations; the identified and actual parameters match, as shown in Table I. Further, a user can inspect the quality of the solution by comparing the measurement data and its estimation, as shown in Fig. 2.

The iteration solution details are presented in Fig. 3. The top figure demonstrates the behavior of the objective function without the regularization term. The middle figure presents the regularization term that approaches zero which indicates the rank constraint is satisfied after 9 iterations. The bottom figure presents each parameter along with iteration steps.

B. A Grid-integrated IBR

The reduced-order analytical model to represent a grid-integrated IBR is from [14], which can offer an explanation on the low-frequency oscillations observed in a real-world wind power plant (WPP) in Texas [15]. In this case study, we adapt the analytical model from [14] into a parameterized structure and identify five parameters.

1) The Analytical Model: The analyzed system is a WPP connected to a grid through a transformer and a transmission shown Fig. 4. The grid is represented with constant voltage magnitude and angle. The line is assumed to be purely induction and the line reactance is notated as X. The point of common coupling (PCC) represents the converter bus that connects the WPP to the grid, where V, P, and Q are the converter voltage magnitude, active power, and reactive power, respectively.

The WPP is treated as a current source. The vector control technique is implemented on the WPP with its d-axis aligned

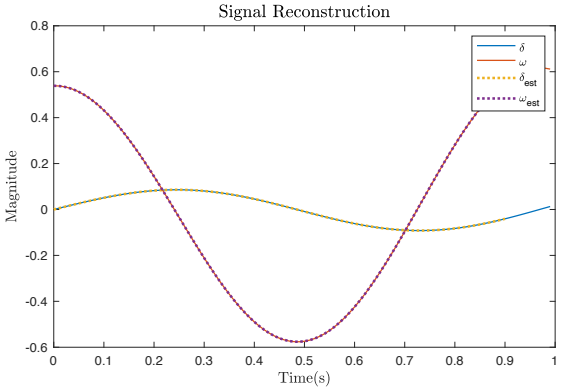

Fig. 2: SMIB impulse data.

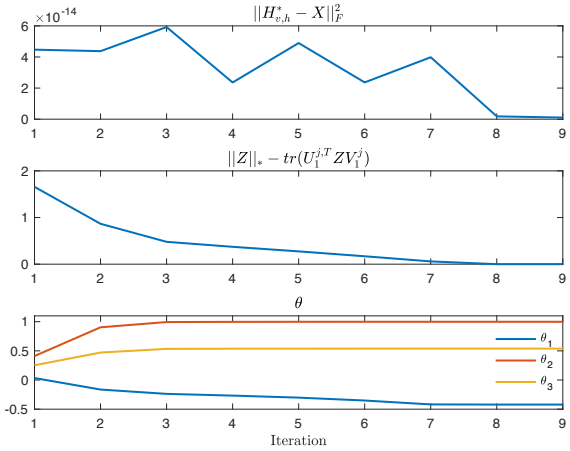

Fig. 3: SMIB solution details.

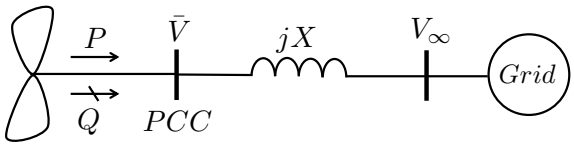

Fig. 4: A wind power plant is connected to the grid.

with the PCC voltage space vector. The WPP's currents, i_d and i_q, can be controlled by two cascaded loops, namely, outer and inner. The d-axis outer loop tracks the real power to generate the d-axis current reference i_d^*, and the q-axis outer control loop tracks the PCC voltage to generate the q-axis current reference i_q^*. The inner current loops track the current references by adjusting the converter output dq-voltages, V_{td} and V_{tq}.

The converter's inner current control is simplified by a first-order system with a time constant τ that takes the reference currents as inputs. The outputs are the dq-axic currents: i_d and i_q.

Since the converter voltage is aligned with the PCC voltage, hence $v_d = V$ and $v_q = 0$. The system's circuit relationship can be expressed as follows in the dq-frame:

$$v_d + jv_q = (jX)\,(i_d + ji_q) + \bar{V}_\infty. \tag{16}$$

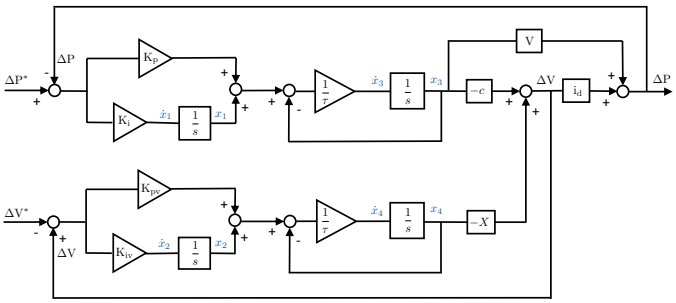

Fig. 5: The WPP linearized analytical model. The model parameter values are $\tau = 0.05, X = 1, i_d = 0.955, K_p = 1, K_i = 1, K_{pv} = 1, K_{iv} = 10, i_{sc} = 1/X, V_d = 1$, and $V_\infty = 1$.

The PCC voltage phase angle, δ, leads the grid voltage's phase angle to ensure the real power flows from the inverter to the grid. The above phasor-based equation can be further decomposed into two equations in real domain.

$$\begin{aligned} v_d &= -Xi_q + V_\infty \cos\delta, \\ v_q &= 0 = +Xi_d - V_\infty \sin\delta. \end{aligned} \tag{17}$$

Note that

$$V_\infty \cos\delta = \sqrt{V_\infty^2 - (V_\infty \sin\delta)^2}, \tag{18}$$

can be plugged in equation (17), which leads to the following

$$v_d = -Xi_q + \sqrt{V_\infty^2 - (Xi_d)^2}. \tag{19}$$

The linearization of (19) gives the following:

$$\Delta V = \Delta v_d = -X\Delta i_q - \underbrace{\frac{X}{\sqrt{\left(\frac{V_\infty}{Xi_d}\right)^2 - 1}}}_{c}\Delta i_d. \tag{20}$$

The active power feeding the grid from the PCC, and its linearized expression is:

$$\begin{aligned} P &= Vi_d, \\ \Delta P &= i_d\Delta V + V\Delta i_d. \end{aligned} \tag{21}$$

The block diagram is shown in Fig. 5.

2) The Analytical Model State-Space: We derive the state-space form of the analytical model to make it compatible with the identification algorithm. The dynamical state of each integrator is indicated in Fig. 5. The state-space form is as follows.

$$\begin{bmatrix} \dot{x}_1 \\ \dot{x}_2 \\ \dot{x}_3 \\ \dot{x}_4 \end{bmatrix} = \underbrace{\begin{bmatrix} 0 & 0 & -K_i\,(V_d - c\,i_d) & K_i X i_d \\ 0 & 0 & -K_{iv}\,c & -K_{iv}\,X \\ \frac{1}{\tau} & 0 & -\frac{K_p(V_d - c i_d)+1}{\tau} & \frac{K_p X i_d}{\tau} \\ 0 & \frac{1}{\tau} & -\frac{K_{pv} c}{\tau} & -\frac{K_{pv} X + 1}{\tau} \end{bmatrix}}_{A} \begin{bmatrix} x_1 \\ x_2 \\ x_3 \\ x_4 \end{bmatrix}$$
$$+ \underbrace{\begin{bmatrix} K_i & 0 \\ 0 & -K_{iv} \\ \frac{K_p}{\tau} & 0 \\ 0 & -\frac{K_{pv}}{\tau} \end{bmatrix}}_{B} \begin{bmatrix} \Delta P^* \\ \Delta V^* \end{bmatrix}. \tag{22}$$

From the above derivation, $(x_1 + K_p(\Delta P^* - \Delta P))$ and $(x_2 + K_{pv}(\Delta V - \Delta V^*)$ are the current orders Δi_d^* and Δi_q^*. x_3 and x_4 are Δi_d and Δi_q, respectively.

3) Model Identification: In this case study, we aim to find five parameters: the time constant, τ, and the controller gains, K_p, K_i, K_{pv}, and K_{iv}, from impulse responses. The operating condition is assumed as known. Hence, v_d, c, i_d, X are all known. We parameterize the system as follows:

$$\mathbf{A}(\theta) = \begin{bmatrix} 0 & 0 & 2.07\theta_2 & 0.955\theta_2 \\ 0 & 0 & -3.22\theta_3 & -\theta_3 \\ \theta_1 & 0 & 2.07\theta_4 - \theta_1 & 0.955\theta_4 \\ 0 & \theta_1 & -3.22\theta_5 & -(\theta_5 + \theta_1) \end{bmatrix},$$
$$\mathbf{B}(\theta) = \begin{bmatrix} \theta_2 & 0 \\ 0 & -\theta_3 \\ \theta_4 & 0 \\ 0 & -\theta_5 \end{bmatrix}. \tag{23}$$

where

$$\theta_1 = \frac{1}{\tau},\ \theta_2 = K_i,\ \theta_3 = K_{iv}$$
$$\theta_4 = \frac{K_p}{\tau},\ \theta_5 = \frac{K_{pv}}{\tau}$$

Assume that all the four states can be measured. We employ the impulse response that is shown in Fig. 6 for the identification process with the sampling time $T = 0.03$ s. Total 100 data points are used. The number of block rows and columns are respectively $v = 10$ and $h = 90$. Compared with the SMIB, this case has a complicated structure and more unknown variables; thus, the global solution is obtained in 82 iterations. Table II shows the identified and actual parameters. It can be seen that the algorithm can recover the accurate parameters.

The iteration details are presented in Fig. 7. The upper subplot shows the total objective function that approaches zero as the solution is found. The bottom subplot presents the parameters over iterations.

TABLE II: Wind Power Plant Analytical Model Parameters.

Parameter	Actual	Estimated
θ_1	20	20.0160
θ_2	1	0.9953
θ_3	10	10.0565
θ_4	20	19.6396
θ_5	20	19.9090

Remark: For both examples, we have demonstrated excellent performance of the proposed method in recovering dynamic model parameters. As the first step, we use a benchmark model's impulse response to recover the parameters of the benchmark model. For future research, we will use measurement data from complicated models to estimate parameters of simplified models.

Remark: A tricky part in DCP problem solving is that the penalty parameter requires trial and error. For the current two examples, the penalty parameter is set as 0.001. We have also found that convergence can be achieved quickly for the first example while it takes many more steps to achieve convergence. Further investigation is necessary.

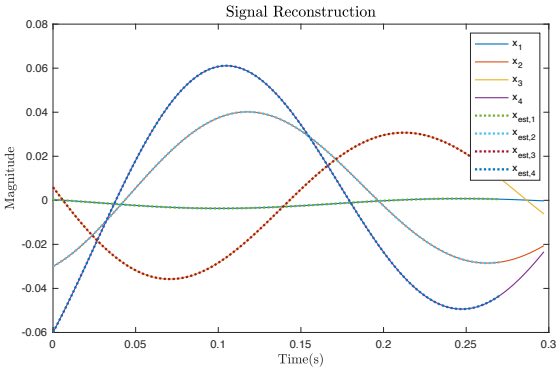

Fig. 6: WPPs impulse data.

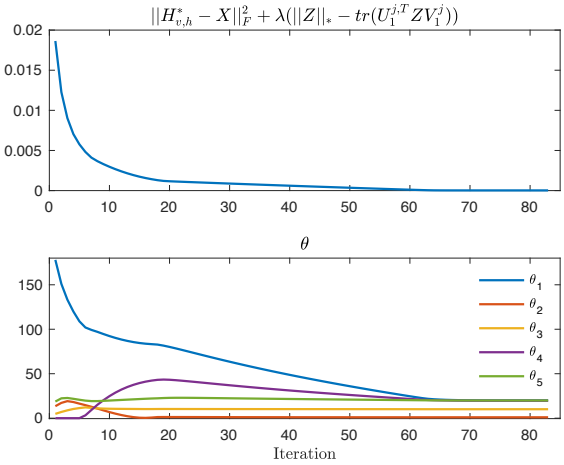

Fig. 7: WPPs iteration solution.

IV. Conclusion

Gray-box model identification is a challenging task since the formulated optimization problems are nonlinear programming problems. Advancements have been made in this area by exploring the low-rank characteristics of the data Hankel matrix and adopting convex programming techniques. This paper adapts the most recent research results of gray-box model identification into synchronous generator parameter identification and IBR parameter identification. Two case studies are used to demonstrate the problem formulation and solving for parameter identification. The results are satisfying for the benchmarked models.

References

[1] P. Pourbeik, A. Ellis, J. Sanchez-Gasca, Y. Kazachkov, E. Muljadi, J. Senthil, and D. Davies, "Generic stability models for type 3 & 4 wind turbine generators for wecc," in *2013 IEEE Power & Energy Society General Meeting*. IEEE, 2013, pp. 1–5.

[2] P. Pourbeik, J. Sánchez-Gasca, J. Senthil, J. Weber, A. Ellis, S. Williams, S. Seman, K. Bolton, N. Miller, R. Nelson *et al.*, "Value and limitations of the positive sequence generic models of renewable energy systems," *This is a brief white-paper prepared by an Ad hoc group within the WECC Renewable Energy Modeling Task Force*, 2015.

[3] "IEEE guide for test procedures for synchronous machines including acceptance and performance testing and parameter determination for dynamic analysis," *IEEE Std 115-2019 (Revision of IEEE Std 115-2009)*, pp. 1–246, 2020.
[4] "IEEE standard procedures for obtaining synchronous machine parameters by standstill frequency response testing," *IEEE Std 115A-1987*, pp. 1–28, 1987.
[5] L. Fan, Z. Miao, S. Shah, P. Koralewicz, V. Gevorgian, and J. Fu, "Data-driven dynamic modeling in power systems: A fresh look on inverter-based resource modeling," *IEEE Power and Energy Magazine*, vol. 20, no. 3, pp. 64–76, 2022.
[6] L. Ljung, "System identification," *Wiley encyclopedia of electrical and electronics engineering*, pp. 1–19, 1999.
[7] L. Fan and Y. Wehbe, "Extended kalman filtering based real-time dynamic state and parameter estimation using pmu data," *Electric Power Systems Research*, vol. 103, pp. 168–177, 2013.
[8] H. G. Aghamolki, Z. Miao, L. Fan, W. Jiang, and D. Manjure, "Identification of synchronous generator model with frequency control using unscented kalman filter," *Electric Power Systems Research*, vol. 126, pp. 45–55, 2015.
[9] C. Yu, L. Ljung, and M. Verhaegen, "Identification of structured state-space models," *Automatica*, vol. 90, pp. 54–61, 2018.
[10] C. Yu, L. Ljung, A. Wills, and M. Verhaegen, "Constrained subspace method for the identification of structured state-space models," *IEEE Transactions on Automatic Control*, 2019.
[11] L. Fan, *Control and dynamics in power systems and microgrids*. CRC Press, 2017.
[12] M. Grant and S. Boyd, "CVX: Matlab software for disciplined convex programming, version 2.1," http://cvxr.com/cvx, Mar. 2014.
[13] J. H. Chow and J. J. Sanchez-Gasca, *Power System Modeling, Computation, and Control*. John Wiley & Sons, 2020.
[14] L. Fan and Z. Miao, "An explanation of oscillations due to wind power plants weak grid interconnection," *IEEE Transactions on Sustainable Energy*, vol. 9, no. 1, pp. 488–490, 2018.
[15] S.-H. Huang, J. Schmall, J. Conto, J. Adams, Y. Zhang, and C. Carter, "Voltage control challenges on weak grids with high penetration of wind generation: Ercot experience," in *2012 IEEE Power and Energy Society General Meeting*. IEEE, 2012, pp. 1–7.